International Journal of Advanced Engineering and Technology Research
ISSN: 3106-8677 (Print), ISSN: 3106-8685 (Online) | Vol. 1, No. 3, 2026

Theoretical Research on Hopf Insulators and Model Construction in One-Dimensional Phononic Crystals

Haoting Zhai

School of Physics and Optoelectric Engineering, Guangdong University of Tecnology, Guangzhou 510006, China

Abstract: In this Letter, a theoretical model of the Hopf insulator is constructed to realize topologically protected boundary states and higher-order corner states via parameter-space modulation. The nontrivial topological order is characterized by the Hopf mapping; by tuning the Hamiltonian coupling parameters, phase transitions are induced, and the localized stability of the boundary and corner states is theoretically verified. Subsequently, this framework is mapped onto a phononic crystal platform, leveraging the tunability of artificial bands to construct a one-dimensional equivalent physical model of the Hopf insulator. Through the precise design of resonator geometries and coupling parameters, an effective correspondence of the topological bands is achieved. Analytical calculations and finite-element simulations exhibit excellent agreement in both band dispersions and eigenstate distributions, confirming the feasibility of this model in acoustic systems and the robustness of its topological states.

Keywords: Condensed Matter of Physics, Topological States of Matter, Hopf insulator, Phononic crystals.

1. Introduction

While conventional topological insulators rely on time-reversal symmetry to maintain phase stability, the evolution of electrons in a magnetic background can drive three-dimensional insulators to exhibit nontrivial band structures, with the Hopf insulator serving as a quintessential theoretical paradigm. In the two-band model, rather than being described by conventional Chern numbers, its topological phase is rigorously characterized by the Hopf invariant, which corresponds to a topological mapping from the three-dimensional momentum space to the two-dimensional sphere. To eliminate Kramers degeneracy, the system must break time-reversal symmetry. Even when all Chern numbers vanish, the bulk of the system remains insulating, yet topologically protected gapless dispersive surface states inevitably emerge at the boundaries. Theoretically, this phase can be physically realized by constructing a tight-binding model incorporating spin-dependent hopping terms. Originating from the momentum-space integral of the gauge field, this invariant endows its nontrivial properties and surface state responses with absolute mathematical and physical robustness, provided that perturbations do not close the bulk gap. Due to its unique topological mechanism, the Hopf insulator has subsequently served as a primary theoretical model for investigating returning Thouless pumps [2, 3], N-band Hopf insulators [4, 5], and non-Hermitian Hopf insulators [6, 7]. In 2023, the first experimental realization of the Hopf insulator in topological circuits were realized [8], marking a pivotal transition in this field from theoretical paradigms to physical implementations.

In this letter systematically elucidates the physical mechanisms of Hopf insulators, as well as their extensions and topological realizations in artificial microstructures. First, grounded in the two-band tight-binding approximation framework of condensed matter physics, this work constructs a theoretical Hamiltonian model to describe the Hopf insulator. At the level of topological characterization, this system is fundamentally defined by the Hopf invariant mapping the three-dimensional momentum space to the two-dimensional Bloch sphere. To thoroughly unveil its bulk-boundary correspondence, we further calculate the projected band structures and the density of states (DOS) profiles under open boundary conditions. The theoretical results not only clearly capture the dispersive topological boundary states traversing the bulk energy gap, but also reveal the localized topological corner states originating from higher-order topological effects. Guided by these theoretical analyses, we further generalize the concept of this topological phase to classical wave systems, carrying out cutting-edge explorations on a phononic crystal platform. Addressing the intrinsic reliance of Hopf insulators on three-dimensional global topological mappings, we innovatively achieve an equivalent realization of the Hopf insulator in a one-dimensional artificial phononic crystal model through a highly exquisite parameter-space coupling design. The band evolution behaviors observed in the phononic crystal are in excellent agreement with the theoretical expectations derived from the preceding Hamiltonian, robustly verifying the accuracy and universality of the theoretical model.

2. Theoretical calculation of Hopf Insulators

The theoretical foundation of Hopf insulators is rooted in the investigation of nontrivial band structures within three-dimensional magnetic insulators [1]. Distinct from conventional topological insulators classified by Chern numbers or Z_2 parity, the Hopf insulator can be realized in its simplest form within a two-band model. Topologically, its physical characteristics are governed by the Hopf invariant, which defines the mapping from the three-dimensional Brillouin zone (T^3) to the Bloch eigenstate space (S^2), corresponding to the third homotopy group $\pi_3(S^2) = \mathbb{Z}$. To lift Kramers degeneracy at time-reversal invariant points, the system must necessarily break time-reversal symmetry. Grounded in the bulk-boundary correspondence, the Hopf insulator in its topologically nontrivial phase hosts protected gapless dispersive surface states at the boundaries. This distinctive topological mapping provides a rigorous

theoretical basis for identifying novel quantum states of matter that lie beyond standard topological classifications, particularly in magnetic systems or engineered coupled frameworks. Synthesizing this theoretical logic with the design requirements for phononic crystal artificial microstructures, we present:

$$\xi_1 = \lambda[sin(k_x) + isin(k_y)]$$

$$\xi_2 = \delta[cos(k_x) - cos(k_y)] + i[M - 2 - tcos(k_x + k_y + k_z)] \quad (1)$$

$$v_i = \xi^{\dagger}\sigma_i\xi \qquad H = \boldsymbol{v}\cdot\boldsymbol{\sigma}$$

Following the formulation of the Hamiltonian matrix, the core task shifts toward verifying the topological response at physical boundaries to elucidate the bulk-boundary correspondence dictated by the Hopf invariant. To visually characterize the topologically protected boundary excitations, we impose open boundary conditions (OBC) along the k_x direction. By projecting the eigenstates onto the surface Brillouin zone, the dispersion characteristics of topological surface states—hidden within the bulk energy gap—can be clearly observed.

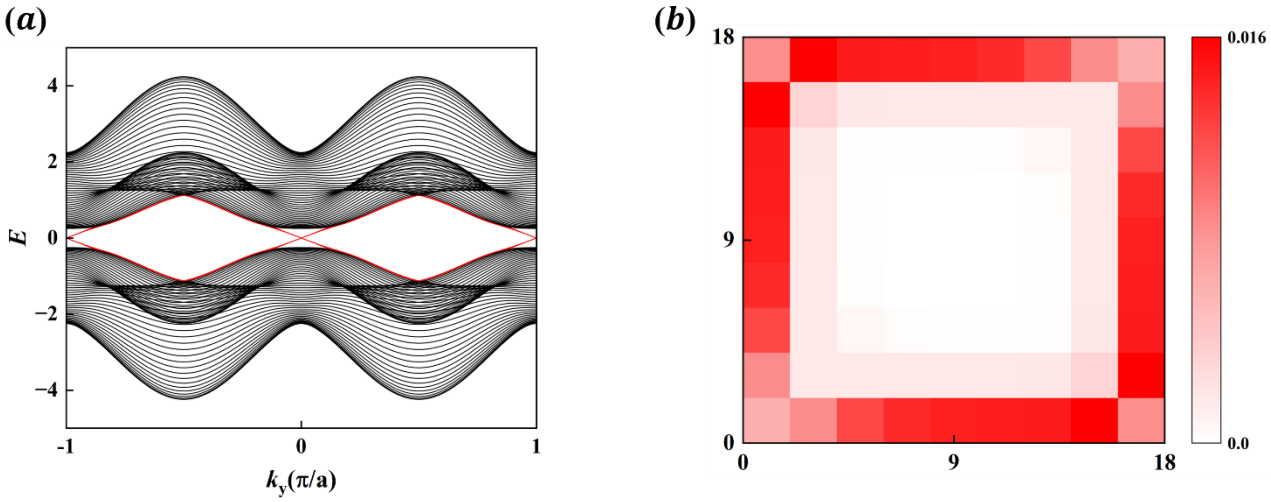

Figure 1. (a) Projected band structure of the Hopf insulator along the k_y direction when $\delta = 0$ under open boundary conditions in the x direction. (b) Corresponding local density of states (LDOS) map of the topological edge states

To further analyze the momentum-space trajectories of these boundary states and their coupling with the bulk, we calculated the projected band structure and density of states (DOS) along the k_y direction for $\delta = 0$, as illustrated in Figure 1. In Figure 1(a), the projected band structure displays typical topological features under the condition $\delta = 0$. It is observed that within the gap formed by the bulk bands, there exist red dispersive branches traversing the energy gap; these curves correspond to boundary excitations protected by the nontrivial Hopf topological invariant. Near $k_y = 0$, the boundary states exhibit characteristic linear or quasi-linear crossings, revealing that the system behaves as a topological phase with Fermi arc-like features under the current parameter set. Figure 1(b) presents the wavefunction probability density $|\psi|^2$ distribution on an 18×18 real-space lattice. Numerical simulations indicate that the states corresponding to the red bands within the gap exhibit strong boundary localization. The concentration of color-coded intensity clearly defines the wavefunctions as residing primarily at the four edges of the system, while the intensity in the bulk region nearly vanishes. This significant boundary localization not only verifies the existence of topological boundary states from a spatial perspective but also complements the in-gap excitations shown in the projected band structure, collectively providing robust evidence for the topological nontriviality of the Hopf model.

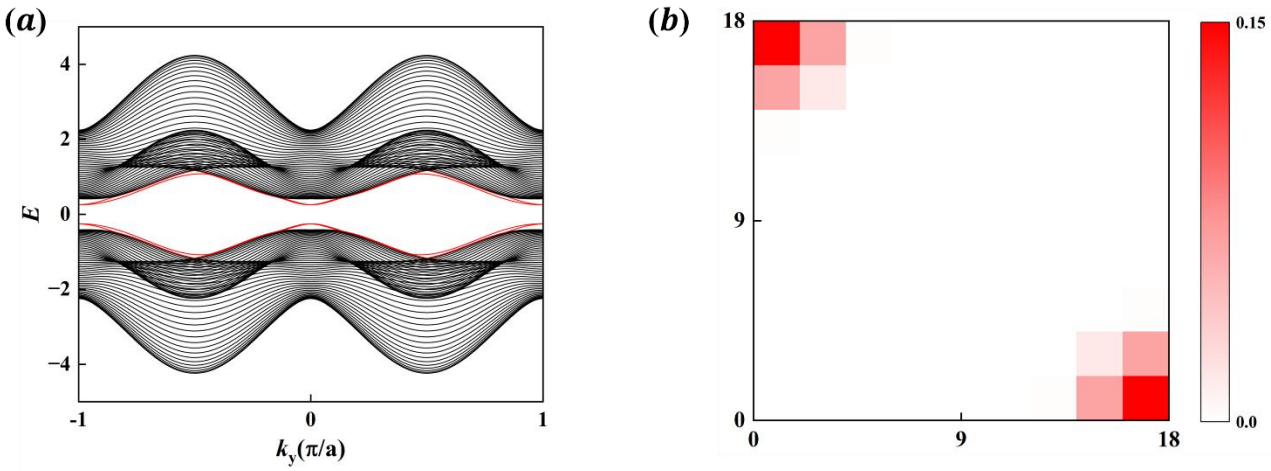

Figure 2. (a) Projected band structure of the Hopf insulator along the k_y direction when $\delta = 0.8$ under open boundary conditions in the x direction. (b) Corresponding local density of states (LDOS) map of the topological edge states

Furthermore, when the parameter δ is increased to 0.8, the topological state of the system undergoes a significant qualitative transition, evolving from a first-order topological phase into a higher-order topological phase. The

corresponding numerical simulation results are illustrated in Figure 2. The other parameter values are set to M = 1.5 and λ = t = 1, which remain unchanged throughout this letter. In the projected band structure shown in Figure 2(a), it can be clearly observed that the gapless Fermi arcs (or edge states) that originally traverse the band gap at δ = 0 are fully gapped out under the influence of the δ term. From a symmetry perspective, the introduction of the δ term breaks the chiral symmetry along the high-symmetry lines, rendering the originally protected edge states unable to maintain their degenerate crossings. However, the opening of this gap does not imply a degradation of the system into a topologically trivial state; rather, it signifies a transition toward a second-order topological insulator. At this stage, although the first-order boundaries (edges) exhibit insulating behavior, the topological properties are further localized into lower-dimensional boundary entities.

The density of states (DOS) distribution in Figure 2(b) intuitively corroborates this higher-order topological feature. In stark contrast to the scenario at δ = 0, where the wavefunctions are dispersively distributed along the entire boundaries, the low-energy eigenstates of the system at δ = 0.8 are highly localized at the four corners of the lattice. The emergence of such topological corner states serves as the central criterion for the second-order topological phase, corresponding to the formation of four zero-energy bound states within the theoretical model. From a topological mathematical perspective, this dimensional transition originates from the reconfiguration of the zero-value contour geometries in momentum space: the original one-dimensional ring-like structures, which previously hindered annihilation, are dismantled by the δ term into four zero-dimensional isolated points, thereby driving the dimensional evolution of the boundary states from one-dimensional edges to zero-dimensional corners.

3. Realization of Hopf insulator in 1D phononic crystal

Within the physical framework of phononic crystals, constructing a three-dimensional Hopf insulator model faces severe constraints in topological mapping and geometric engineering challenges in real space. Although Yan and his research group have successfully achieved the experimental observation of three-dimensional Hopf insulators by leveraging the highly reconfigurable nature of circuit systems [8], physical realizations in continuous-medium systems, such as acoustics, remain exceedingly difficult. The core dilemma stems from the contradiction between the unique mathematical structure of the Hopf insulator and its physical representation in real space: the distinctive Hopf mapping mechanism dictates that its effective Hamiltonian, in the minimal model, consists solely of a 2 × 2 matrix; however, to establish a nontrivial Hopf topological invariant, the components of this Hamiltonian must encompass complex momentum terms containing higher-order Fourier components.

Under the tight-binding approximation, this implies that each lattice site requires not only intricate intracell spin-orbit coupling but also a multitude of spinor-dependent hopping terms extending across nearest and even next-nearest neighbors. In phononic crystals, every hopping coupling must be physically realized through acoustic coupling channels or connecting rods. Due to the limited geometric volume of a phononic crystal unit cell, such high-density coupling requirements severely compress the available spatial leeway within the cell. An excessive number of coupling rods not only generates severe physical interference, encroaching upon the intrinsic space of the acoustic resonators, but also risks reaching a fabrication limit where the finite unit cell volume cannot accommodate all the necessary topological coupling structures. Furthermore, complex physical connections inevitably introduce non-negligible parasitic modal couplings, which degrade the purity of the topological bands.

To address this engineering bottleneck of real-space coupling saturation, this subsection adopts a dimensional reduction strategy. By projecting the topological mechanism described by Eq.1 down to a one-dimensional space for a reduced-dimensional analysis, this approach aims to simplify the complexity of spatial routing, thereby thoroughly exploring and verifying the unique coupling configurations and the underlying topological dynamics of this system. Building upon the preceding discussion, we set $k_y = k_z = 0$ in Eq.1 to obtain the one-dimensional (1D) Hopf insulator Hamiltonian H_{1D}, which takes the following explicit form:

$$H_{1D} = \begin{pmatrix} A & B \\ B^* & -A \end{pmatrix} \tag{2}$$

Where: $A = -0.25 - \delta^2 - \cos(k_x) + 2\delta^2\cos(k_x) - cos^2(k_x) - \delta^2 cos^2(k_x) + sin^2(k_x)$ and $B = -2\,\delta\sin(k_x) + 2\,\delta\cos(k_x)\sin(k_x) + i\,(\sin(k_x) + 2\cos(k_x)\sin(k_x))$. It should be particularly noted that the physical interactions encompassed in Eq. 2 can be systematically categorized into five types based on their coupling mechanisms and algebraic characteristics: regular coupling, lossy coupling, gain-type coupling, and positive and negative couplings with opposite polarities. Despite the introduction of terms such as "gain" and "loss" in the physical description, it would be theoretically imprecise to hastily classify this Hopf insulator model within the domain of non-Hermitian physics.

An analysis of the effective Hamiltonian matrix construction reveals that the off-diagonal terms strictly follow a conjugate symmetric distribution (e.g., the $\pm i$ components within the σ_y term), and the diagonal elements remain real, containing no complex terms that would represent asymmetric energy exchange. According to the rigorous definition of Hermitian operators, the matrix satisfies the operator identity $H - H^\dagger = 0$, ensuring that the system remains firmly within the Hermitian framework at the level of band topological classification.

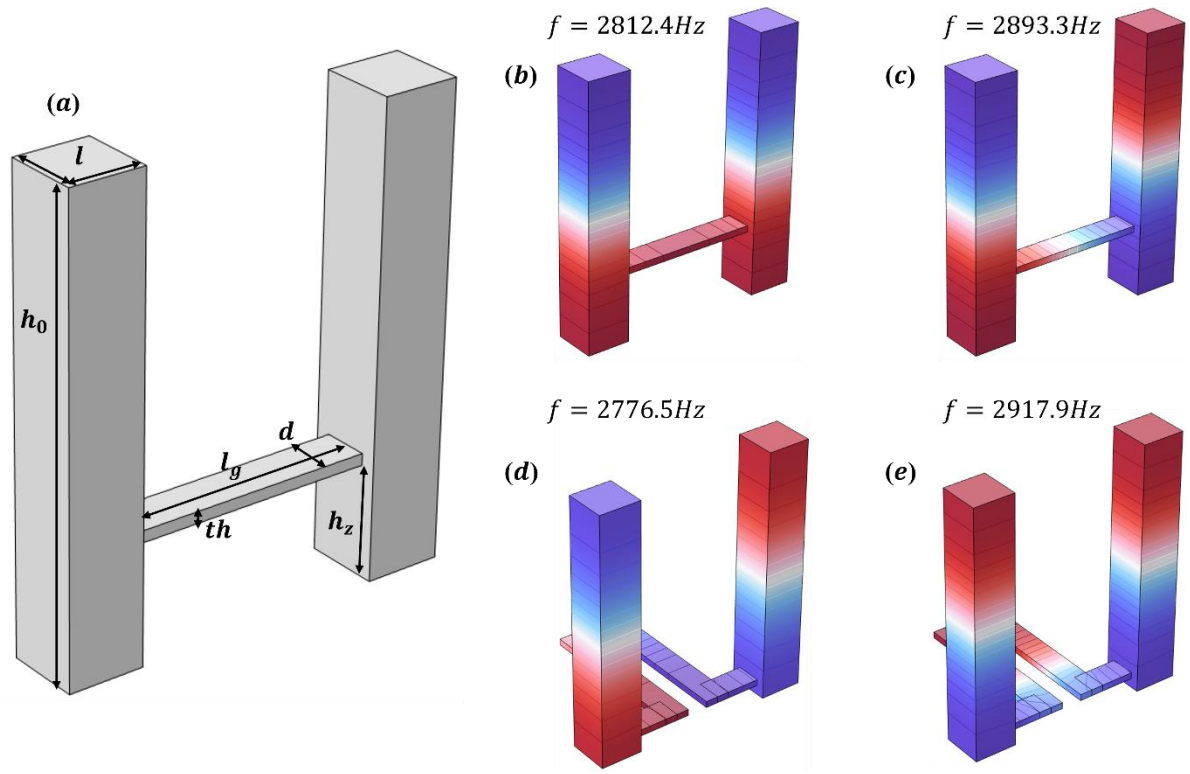

Figure 3. (a) Schematic diagram of the acoustic cavities and coupling parameters. (b) In-phase sound pressure distribution for nearest-neighbor negative coupling. (c) Out-of-phase sound pressure distribution for nearest-neighbor negative coupling. (d) Out-of-phase sound pressure distribution for nearest-neighbor positive coupling. (e) In-phase sound pressure distribution for nearest-neighbor positive coupling

Due to the emergence of second-order terms, we designed four types of couplings: two pairs of positive and negative couplings for nearest-neighbor and next-nearest-neighbor interactions. In the acoustic tight-binding model, the sign of the coupling coefficient κ is strictly defined by the modal phase relationships following the splitting of degenerate energy levels. Consider a dimer system of two identical resonators with eigenfrequency ω0; the introduction of a real coupling coefficient κ splits the system into two characteristic frequencies $\omega_{\pm} = \omega_0 \pm \kappa$, corresponding to in-phase and out-of-phase modes. Negative coupling (κ < 0) occurs when the in-phase mode frequency is lower than the out-of-phase mode. Conversely, positive coupling (κ > 0) is defined when the in-phase mode frequency is higher [9,10].

In phononic crystals, realizing such a dimer requires geometric anisotropy. Practically, increasing the z-height breaks the spherical symmetry, evolving the eigenmode from a spatially uniform s-orbital (monopole) to a directional P_z-orbital (dipole). Once the geometry is fixed, the eigenfrequency f_0 serves as the reference. The coupling sign is rigorously determined by the frequency response: if the in-phase frequency f_{even} is higher than the out-of-phase frequency f_{odd} ($f_{even} - f_{odd} > 0$), the coupling is positive (κ > 0); otherwise, it is negative (κ < 0).

Figure 3(a) illustrates the schematic and key geometric parameters of the acoustic resonator and coupling rod. The acoustic unit cell consists of a rectangular resonator with height h0 and cross-section l × l. Based on the wave equation, the eigenfrequency is defined as $f_0 = \frac{c_0}{(2h_0)} = 2853$ Hz, serving as the core reference for constructing topological bands. The design utilizes the first-order longitudinal standing wave mode (P_z dipole mode), where the internal pressure distribution follows $P(x,y,z) = P_0 \cos\left(2\pi \frac{h_z}{h_0}\right)$.

When the coupling rod is attached at position h_z, the coupling strength κ is modulated by the rod's cross-section (width d and thickness th). Crucially, the rod length lg determines the coupling polarity. By selecting $l_g = h_0(n - 0.5)$ (where n is a positive integer), the phase delay during transmission is precisely controlled. This ensures that the in-phase and out-of-phase modes split around f_0, enabling independent definition of positive and negative couplings. As shown in Figures 3(b)-(c), for $l_g \approx 0.5h_0$, the out-of-phase frequency is significantly higher than the in-phase frequency, identifying it as nearest-neighbor negative coupling. Conversely, in Figures 3(d)-(e) where $l_g \approx 1.5h_0$, the in-phase frequency is higher, representing nearest-neighbor positive coupling.

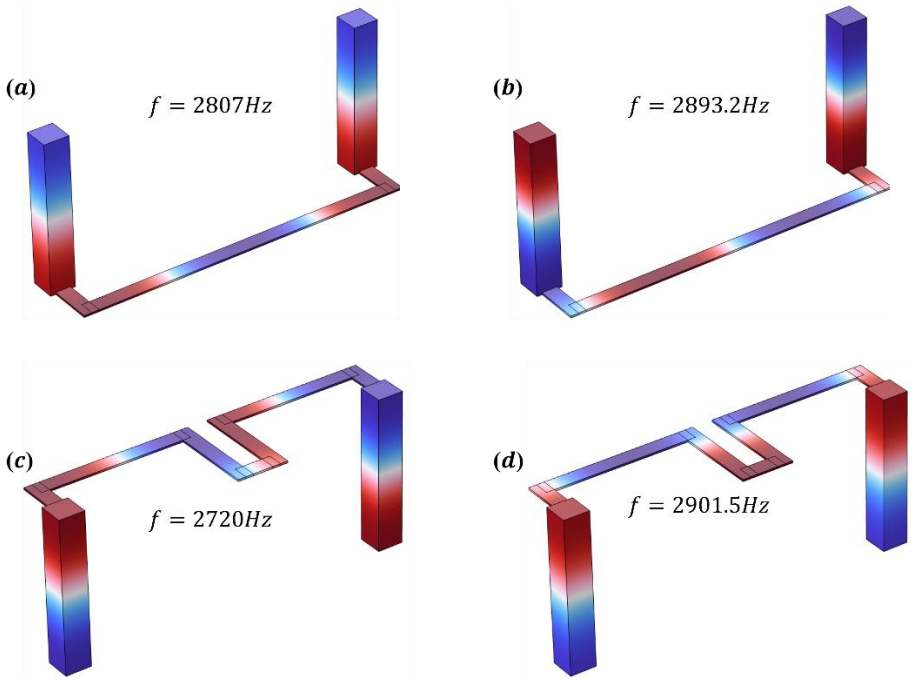

Figure 4. (a) In-phase sound pressure distribution for next-nearest-neighbor negative coupling. (b) Out-of-phase sound pressure distribution for next-nearest-neighbor negative coupling. (c) Out-of-phase sound pressure distribution for next-nearest-neighbor positive coupling. (d) In-phase sound pressure distribution for next-nearest-neighbor positive coupling

When the coupling rod length is set to $l_g = 2.5h_0$, as shown in Figures 4(a) and 4(b), the system exhibits significant positive coupling characteristics. In this configuration, the symmetry modes of the dimer system undergo characteristic splitting: the eigenfrequency of the in-phase mode shifts to 2893.2 Hz, exceeding the intrinsic reference frequency f0, and displays a distinct high-frequency shift relative to the out-of-phase mode frequency of 2807.0 Hz. As the connecting rod length is further increased to $l_g = 3.5h_0$, as shown in Figures 4(c) and 4(d), the phase delay accumulated within the transmission channel undergoes a shift of an odd multiple of π, causing the frequency response to exhibit a completely inverted evolution trend. In this state, the energy levels evolve in reverse: the in-phase mode eigenfrequency of 2720.0 Hz falls below the out-of-phase mode frequency of 2901.5 Hz. Furthermore, their polarity shifts relative to f0 are inverted, marking the system's successful transition to negative coupling. This real-space verification, based on the design logic $l_g = h_0(n - 0.5)$, strictly echoes the previously discussed phase control strategy.

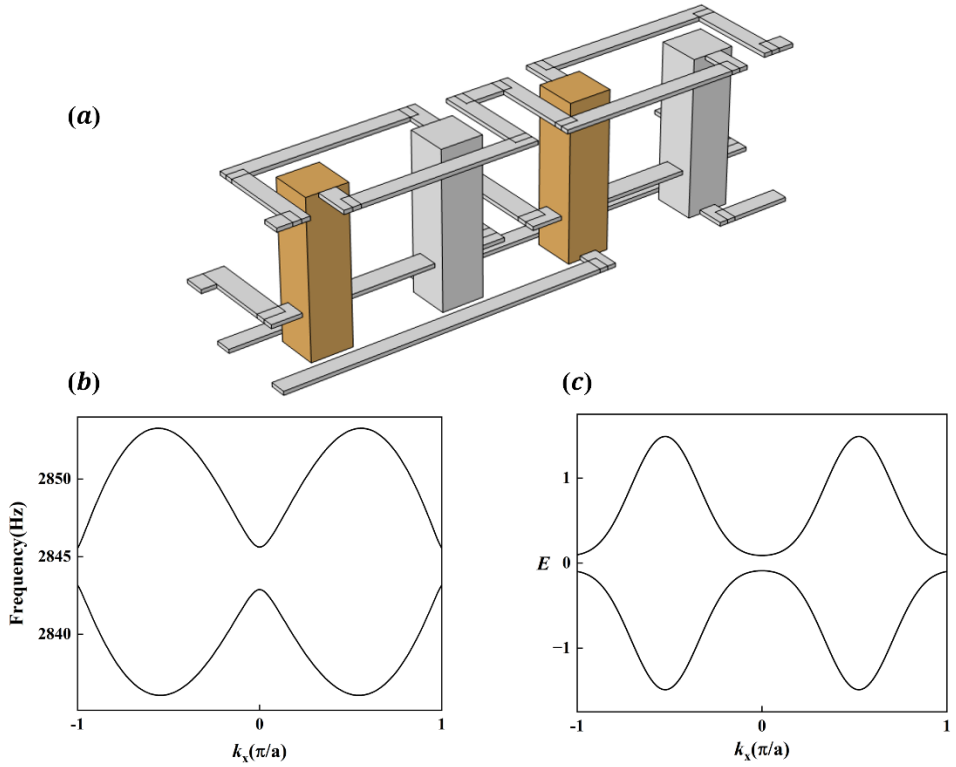

Figure 5. (a) Unit cell model of a one-dimensional Hopf insulator. (b) Simulated band structure along the (k_x) direction. (c) Theoretically calculated band structure along the (k_x) direction

Following the systematic validation of the resonator modal properties and the positive/negative coupling mechanisms, this work establishes the theoretical and structural foundation for constructing the one-dimensional Hopf insulator phononic crystal model. Given the complex next-nearest-neighbor couplings and specific phase winding features inherent to this topological model, a unit cell comprising four acoustic resonators is employed to precisely map the topological properties of the Hamiltonian in real space. As illustrated in Figure 5(a), the yellow and gray cavities represent the A and B sublattice degrees of freedom, respectively, serving as physical carriers to simulate the two-band system. The intra- and inter-cell topological connection strategies strictly adhere to the geometric coupling criteria established in Figures 3 and 4. By precisely tuning the phase delay and impedance matching of the connecting rods, the acoustic hopping coefficients are maintained highly consistent with the theoretical model in both magnitude and polarity.

Figures 5(b) and 5(c) display the projected band structures along the k_x direction, obtained via finite-element simulations and tight-binding calculations, respectively. A comparative analysis reveals that the simulated band evolution trajectories, along with the gap positions and widths, exhibit excellent agreement with the theoretical results. This remarkable consistency not only verifies the precise reproduction of the Hopf topological phase by the 1D artificial microstructure at the bulk band level, but also lays the groundwork for generalizing the Hopf insulator to higher-dimensional phononic crystal models.

4. Summary

This letter systematically establishes the theoretical framework of the Hopf insulator and physically realizes it via artificial microstructures. Topologically characterized by the Hopf mapping from a 3D to a 2D sphere, we utilize a tight-binding model to reproduce Fermi arc surface states and induce a transition to a higher-order topological phase with localized corner states, mathematically confirming the robust bulk-boundary correspondence.

To overcome spatial and geometric constraints in 3D phononic crystals, we apply a dimensional reduction strategy, mapping the 3D Hopf Hamiltonian onto a 1D acoustic lattice. By employing highly anisotropic cavities, we break spherical symmetry to transition the eigenmode from a uniform s-orbital to a polarized P_z dipole orbital. Specific coupling rod lengths are designed to independently construct positive and negative couplings in real space, overcoming traditional acoustic limitations. The excellent agreement between simulated and theoretical band structures robustly verifies our 1D model. This research advances the understanding of higher-order Hopf states and establishes a novel paradigm for manipulating high-dimensional topological invariants in low-dimensional systems for advanced acoustic applications.

References

[1] MOORE J E, RAN Y, WEN X G. Topological surface states in three-dimensional magnetic insulators [J]. Physical review letters, 2008, 101(18): 186805.

[2] ZHU P, ZHANG R X. Delicate topology of Luttinger semimetal [J]. Physical Review B, 2024, 110(16): 165120.

[3] ZHU P, ALEXANDRADINATA A, HUGHES T L. Z 2 spin Hopf insulator: Helical hinge states and returning Thouless pump [J]. Physical Review B, 2023, 107(11):115159.

[4] LAPIERRE B, NEUPERT T, TRIFUNOVIC L. N-band Hopf insulator [J]. Physical Review Research, 2021, 3(3): 033045.

[5] LENG B, VAN V. N-band photonic Hopf insulators based on 2D microring lattices [J]. Optics Letters, 2022, 47(19): 5128-5131.

[6] PAK S, YEOM C H, VERMA S, et al. PT-symmetric non-Hermitian Hopf metal [J]. Physical Review Research, 2024, 6(1): L012053.

[7] NAKAMURA D, KAWABATA K. Non-Hermitian Hopf insulators [J]. Physical Review B, 2025, 112(7): 075134.

[8] WANG Z, ZENG X T, BIAO Y, et al. Realization of a Hopf insulator in circuit systems [J]. Physical review letters, 2023, 130(5): 057201.

[9] QI Y, QIU C, XIAO M, et al. Acoustic realization of quadrupole topological insulators [J]. Physical Review Letters, 2020, 124(20): 206601.

[10] WU S Q, CHENG W, LIU X Y, et al. Observation of d-class topology in an acoustic metamaterial [J]. Science Bulletin, 2024, 69(7): 893-900.